Assessing Polarimetric Weather Radar Data Quality Under Cross-Polar Coupling and Sampling Limits

Heylen, J.; Dash, T.; Theis, G.; Meer, R. van der; Aslan, Y.; Yarovoy, A.

DOI
10.1109/RadarConf2559087.2025.11205140

Publication date
2025

Document Version
Final published version

Published in
Proceedings of the 2025 IEEE Radar Conference, RadarConf 2025

Assessing Polarimetric Weather Radar Data Quality Under Cross-Polar Coupling and Sampling Limits

Jonas Heylen
Robin Radar Systems, NL
Microelectronics, TU Delft
jonasheylen@tudelft.nl

Tworit Dash
Microelectronics, TU Delft
t.k.dash@tudelft.nl

Guilherme Theis
Robin Radar Systems, NL
guilherme.theis@robinradar.com

Rob van der Meer
Robin Radar Systems, NL
rob.vandermeer@robinradar.com

Yanki Aslan
Microelectronics, TU Delft
y.aslan@tudelft.nl

Alexander Yarovoy
Microelectronics, TU Delft
a.yarovoy@tudelft.nl

2025 IEEE Radar Conference (RadarConf25) | 979-8-3315-4433-1/25/$31.00 ©2025 IEEE | DOI: 10.1109/RADARCONF2559087.2025.11205140

***Abstract*—The impact of cross-polar coupling and a finite available number of echo samples on the data quality of polarimetric weather radar data is investigated. A system model and a two-step simulation approach are proposed to simulate realistic time series of the received weather radar signals. The proposed simulation methodology is applied to a rainfall scenario to illustrate the data quality of two widely used weather radar measurement schemes. Through simulation of the bounds within which 90% of the resulting estimates fall, it is demonstrated that the finite sample size introduces deviations that limit the data quality, even in designs with low cross-polar coupling.**

***Index Terms*—Data quality, polarimetry, polarimetric coupling, weather radar.**

I. Introduction

Real-time information on crucial parameters related to the weather is essential not only for predicting climate patterns in the future, but also for immediate applications such as aviation safety. Among atmospheric phenomena, heavy precipitation has significant implications, especially for flood risk management. Hydrometeor classification and *Quantitative Precipitation Estimation* (QPE) are necessary to assess such extreme weather events. Modern *Polarimetric Phased-Array Radars* (PPAR) are becoming increasingly popular nowadays for quantitatively measuring such events instantaneously in space (because of their electronic scanning nature) and their ability to gather information on hydrometeor shape and orientation due to the polarimetric feature [1]. However, there are two major challenges when it comes to the polarimetric data quality: coupling between the different polarizations, resulting in non-zero *Cross-Polarization Discrimination* (XPD), and a finite number of available samples.

The XPD problem is illustrated in Fig. 1. The illustration clarifies that even for a simple dual-polarized antenna element comprising two orthogonal dipoles, the directions of the radiated electric fields will not be orthogonal off the broadside. The intended polarizations in weather radar are defined in the *horizontal* (H) / *vertical* (V) polarization basis. As shown in Fig. 1, these correspond to the ϕ (azimuth) and negative θ (elevation) vectors in spherical coordinates. This linear dual-polarization scheme has become the most commonly used because it reduces the propagation effects on the polarization state of the wave [2, Ch. 2, pp.19-20].

This research was supported by the National Growth Fund through the Dutch 6G flagship project "Future Network Services".

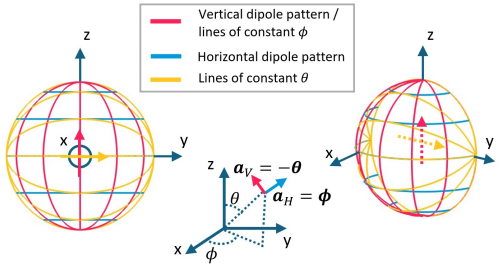

Fig. 1. Non-orthogonal emitted fields by two orthogonal dipoles. The coordinate system shows the convention commonly used for the weather radar.

The second major polarimetric data quality challenge of interest is the finite number of echo samples available in time for practical scanning weather radar configurations. The radar echoes in time, encapsulating the radial motion of many hydrometeors in large volumes, are usually characterized by stochastic random processes. This correlated random process in time indicates an extended Doppler spectrum in frequency (usually described with a Gaussian shape), capturing the motion of all the hydrometeors [3, Ch. 4, pp.67-68], [4, Eq. (1)-(6)]. The random nature of the received signal implies the statistics of the estimators should be studied, as they limit the data quality.

Previous works have studied these two major challenges separately. When investigating the bias due to cross-polar coupling [5], [6], higher-order coupling terms are usually neglected to achieve closed-form analytical formulae for this bias. As for the effect of a finite number of echo samples, the characterization of the standard deviation of polarimetric estimates has received a lot of attention [7], [8], [9]. Usually, perturbation analysis is used to linearize the distributions. However, this method is limited to small variations. Further-

more, the estimated polarimetric variables are not distributed according to a normal distribution [7, Ch. 5], with the exception of the received power, in linear scale, for a single polarization and a large echo record. The bias and standard deviation are thus not sufficient to characterize the distribution of the estimated quantities.

This paper proposes a simulation methodology to study these challenges, resulting in the following novel contributions:

- Data quality reduction due to both cross-coupling and a finite number of echo samples is studied simultaneously,
- Through a Monte Carlo approach, the bounds within which the estimated polarimetric quantities will fall in realistic weather scenarios are obtained.

The higher-order coupling terms are not neglected in this work. The two most popular measurement schemes are compared: the *alternate transmit* (AHV) and *simultaneous transmit* (SHV) approach. In SHV mode, both H and V are emitted simultaneously. In AHV mode, H and V are transmitted alternately on a pulse-to-pulse basis. Simultaneous reception of both polarizations is implied in both modes.

The remainder of the paper is organized as follows. Section II explains the methodology and the simulation strategies. Section III explains the simulation results. Finally, Section IV concludes the paper.

II. Methodology

To simulate the combination of the bias introduced by cross-polar coupling, as well as the statistical variability introduced by the nature of weather radar signals, the simulation will be carried out in two different steps. First, the expected values of the polarimetric estimates are modeled. Secondly, the Doppler spectrum is taken into account to simulate realistic time series of the received voltages. Using a Monte Carlo simulation, an empirical distribution of the estimated variables can be calculated. This distribution can then be used to calculate the bounds within which these estimated variables will fall. In Section III, this method will be demonstrated to calculate the bounds within which the estimates will be in $90\,\%$ of cases for a specific rainfall scenario.

A. System model and expected covariance matrices

To simulate a realistic received polarimetric weather signal, the expected values of the received covariance matrices need to be defined. In this work, the approach is based on [10], where a method is introduced to separate the effects of the antenna patterns from the effects of scattering. Although the approach to simulating covariances for the SHV mode is the same as in [10], the approach taken to simulate the AHV mode differs. This can be seen, starting from the weather radar equation:

$$\begin{bmatrix} V_H \\ V_V \end{bmatrix} = C(r_0) \sum_{i=1}^{N} e^{-\gamma_0 \hat{k}.\Delta\overline{r_i}} \cdot \mathbf{F}_r \cdot \mathbf{S} \cdot \mathbf{F}_t \cdot \mathbf{U}_{a\to HV} \cdot \begin{bmatrix} 1 \\ 0 \end{bmatrix}, \quad (1)$$

where $C(r_0)$ is a range-dependent constant due to propagation, $\mathbf{F}_t$ and $\mathbf{F}_r$ denote the antenna pattern matrices on transmit and receive, respectively, and $\mathbf{S} = \begin{bmatrix} s_{hh} & s_{hv} \\ s_{hv} & s_{vv} \end{bmatrix}$ denotes the scattering parameters, where reciprocity is assumed. The wave propagation vector is denoted by $\hat{k}$ and $\Delta\overline{r_i}$ is the vector from the center of the resolution volume to the hydrometeor. Finally, $\mathbf{U}_{a\to HV}$ denotes the expression of the transmitted polarization in the H/V basis. The transmitted polarization is either H or V for the AHV mode, and the combination of H and V for the SHV mode. It is assumed here that the same antenna is used for transmission and reception, and thus $\mathbf{F}_r = \mathbf{F}_t^T$. The antenna is modeled as in [5]:

$$\mathbf{F}_t = \begin{bmatrix} 1 & \delta \cdot e^{j\gamma_{hv}} \\ \delta \cdot e^{j\gamma_{vh}} & 1 \end{bmatrix}, \quad (2)$$

where δ is defined in terms of the one-way XPD of the antenna as:

$$\mathrm{XPD} = 20 \cdot \log_{10}(\delta) \quad \mathrm{dB}, \quad (3)$$

and γ denotes the phase of the cross-polar patterns, relative to the co-polar patterns. These are assumed to be perfectly calibrated, implying no amplitude or phase differences between the co-polar H and V patterns.

Consider a transmitted polarization a_1 resulting in the samples at slow-time index m, and a transmitted polarization a_2 resulting in samples at index $m + l$. The following assumptions are made [10]: the neglect of multiple scattering, a large distance to the center of the radar resolution volume compared to the resolution volume dimensions, and statistical homogeneity of the scattering characteristics. Utilising the vectorization operator and Kronecker product, the resulting expected values of the received voltage covariance matrix can then be written as follows:

$$\begin{aligned} \mathrm{vec}\left(\mathbb{E}\left\{\begin{bmatrix} V_H[m] \\ V_V[m] \end{bmatrix}\begin{bmatrix} V_H^*[m+l] & V_V^*[m+l] \end{bmatrix}\right\}\right) = \\ C_{\mathrm{tot}}(r_0) \cdot \mathbf{Q}_{\mathrm{tot}} \cdot \mathbf{U}_{\mathrm{tot}} \cdot \mathbf{F}_{\mathrm{tot}} \\ \cdot \mathbb{E}\left\{\mathrm{vec}(\mathbf{S_v}[m] \cdot \mathbf{S_v}[m+l])^H) \cdot e^{-j\frac{4\pi}{\lambda} v_r l T_s}\right\}, \quad (4) \end{aligned}$$

where $C_{\mathrm{tot}}(r_0)$ is the constant including range effects,

$$\mathbf{Q}_{\mathrm{tot}} = \left(\begin{bmatrix} 1 & 0 \end{bmatrix} \otimes \begin{bmatrix} 1 & 0 \\ 0 & 1 \end{bmatrix}\right) \otimes \left(\begin{bmatrix} 1 & 0 \end{bmatrix} \otimes \begin{bmatrix} 1 & 0 \\ 0 & 1 \end{bmatrix}\right), \quad (5)$$

$$\mathbf{U}_{\mathrm{tot}} = \left(\mathbf{U}_{a\to HV}^T \otimes \begin{bmatrix} 1 & 0 \\ 0 & 1 \end{bmatrix}\right)^* \otimes \left(\mathbf{U}_{a\to HV}^T \otimes \begin{bmatrix} 1 & 0 \\ 0 & 1 \end{bmatrix}\right), \quad (6)$$

$$\mathbf{F}_{\mathrm{tot}} = \left(\mathbf{F_t}^T \otimes \mathbf{F_r}\right)^* \otimes \left(\mathbf{F_t}^T \otimes \mathbf{F_r}\right), \quad (7)$$

$$\mathbf{S_v} = \mathrm{vec}\left(\mathbf{S}\right). \quad (8)$$

The reader is referred to [10] for the derivation method, where the equations for the case of $a_1 = a_2$, $l = 0$, and for a generic polarization basis are derived. The authors of [10] also propose a way to include propagation effects, which is outside the scope of this paper. Finally, it is assumed that the velocity distribution is independent of those for size, shape, and orientation [7, Ch. 5, pp.240] and that the distribution of

the scattering parameters remains constant over the dwell time. This allows to simplify the last term of (4) as:

$$\mathbb{E}\left\{\mathrm{vec}(\mathbf{S_v}[m]\cdot\mathbf{S_v}[m+l]^H)\cdot e^{-j\frac{4\pi}{\lambda}v_r l T_s}\right\} = \mathbb{E}\left\{\mathrm{vec}(\mathbf{S_v}[m]\cdot\mathbf{S_v}[m+l]^H)\right\}\cdot\mathbb{E}\left\{e^{-j\frac{4\pi}{\lambda}v_r l T_s}\right\}. \quad (9)$$

To simulate weather targets in a realistic way, different techniques can be used to get the expected values of the scattering parameters, which are the inputs to the system model presented in this paper. In principle, these can be calculated based on sophisticated numerical methods, combined with inputs from numerical weather prediction models [11], to model one specific real-world weather event. However, in this work these will be selected based on a representative rainfall scenario to demonstrate the applicability of the proposed method.

The final term in (9) is related to the velocity distribution. A Gaussian spectrum is usually assumed [4]. In this case, the expected value from (9) results in:

$$\mathbb{E}\left\{e^{-j\frac{4\pi}{\lambda}v_r l T_s}\right\} = e^{-j\frac{4\pi}{\lambda}v_{r,m} l T_s}\cdot e^{-\frac{8\pi^2}{\lambda^2}\sigma_v^2 l^2 T_s^2}, \quad (10)$$

where $v_{r,m}$ [m/s] is the mean radial velocity of the hydrometeors in the resolution volume, λ [m] is the wavelength, l is the lag between the pulses under consideration, T_s [s] is the pulse interval time, and σ_v [m/s] is the spectral width [7, Ch. 5]. It represents the width of the radial velocity spectrum, and is a measure of the velocity dispersion. In this work, a zero-mean radial velocity is assumed for simplicity. In practice, this is a relevant case: one can imagine a radar pointing towards the horizon, where the raindrops can have a zero mean velocity towards the radar in the absence of wind fields. In that case, (10) can be written in terms of the normalised spectral width $\sigma_{vn} = \frac{2\sigma_v T_s}{\lambda}$.

Hence, the resulting expression used to simulate the expected values of the covariance matrices is as follows:

$$\mathrm{vec}\left(\mathbb{E}\left\{\begin{bmatrix}V_H[m]\\V_V[m]\end{bmatrix}\begin{bmatrix}V_H^*[m+l] & V_V^*[m+l]\end{bmatrix}\right\}\right) \quad (11)$$
$$= C_{\mathrm{tot}}\cdot\mathbf{Q}_{\mathrm{tot}}\cdot\mathbf{U}_{\mathrm{tot}}\cdot\mathbf{F}_{\mathrm{tot}}\cdot\mathbb{E}\left\{\mathrm{vec}(\mathbf{S_v}\cdot\mathbf{S_v}^H)\right\}\cdot e^{-2\cdot(\pi\sigma_{vn}l)^2}.$$

These covariance matrices can now be used to determine the cross-polarization induced bias in the expected values of the polarimetric variables. The estimators used in this paper are based on estimations of these covariance matrices [7, Ch. 6, pp.342-348]:

$$\hat{\mathbf{Z}}_{HH} \propto 10\cdot\log_{10}\left(\frac{1}{M}\sum_m |V_H[m]|^2\right) \quad \mathrm{dB}, \quad (12)$$

$$\hat{\mathbf{Z}}_{DR} = 10\cdot\log_{10}\left(\frac{\sum_m |V_H[m]|^2}{\sum_m |V_V[m]|^2}\right) \quad \mathrm{dB}, \quad (13)$$

where the co-polar samples are used for these estimators, being all the received samples for the SHV mode. A hat ($\hat{}$) diacritic on any variable indicates that it is an estimated quantity. For the AHV mode, only indices $2m$ are used for the H and $2m+1$ for the V polarization. As for the co-polar correlation coefficient, estimators differ for the SHV and AHV modes. For SHV:

$$\hat{\rho}_{HV}^{SHV} = \left|\frac{\sum_m V_H^*[m]\cdot V_V[m]}{\sqrt{\sum_m |V_H[m]|^2\sum_m |V_V[m]|^2}}\right| \quad (14)$$

In AHV mode, however, the available co-polar samples have a one-pulse time delay between them. The simple estimator proposed by [12] is utilised here:

$$\hat{\rho}_{HV}^{AHV} = \frac{\left|\frac{\sum_m V_H^*[2m]\cdot V_V[2m+1]}{\sqrt{\sum_m |V_H[2m]|^2\sum_m |V_V[2m]|^2}}\right|}{\left|\frac{\sum_m V_H[2m]\cdot V_H^*[2m+2]}{\sum_m |V_H[2m]|^2}\right|^{0.25}}, \quad (15)$$

which is seen to be the estimation of the correlation between the co-polar samples with a lag one delay, divided by the estimation of the autocorrelation coefficient.

Other variables, such as the *linear depolarization ratio* (LDR) and the differential phase are not estimated. The LDR can not be estimated in the SHV mode, and the unambiguous interval in which the differential phase can be estimated is half as large in the SHV mode when compared to the AHV mode [7, Ch. 6]. As such they are omitted here to allow for a fair comparison between the modes.

The expected values of these estimators can now be calculated based on elements of the different covariance matrices (11). The bias resulting from the cross-polar coupling will depend not only on the antenna patterns but also on the target variables. It should be noted that three variables remain arbitrary in this work: the phases of the cross-polar patterns (γ_{hv}, γ_{vh}), since they are often unknown, and the differential phase (angle of $< s_{hh}^* s_{vv} >$), as this is an accumulating variable that can take on different values in the same weather event, depending on the distance of the resolution volume to the radar. The simulation therefore loops through all possible combinations in this phase space to find the worst-case bias, as proposed in [5]. Both the maximum positive bias and the minimum negative bias are calculated,, which can be translated into QPE accuracies using different models of the rainfall rate [2, Ch. 7], [7, Ch. 8].

B. Time-series simulation

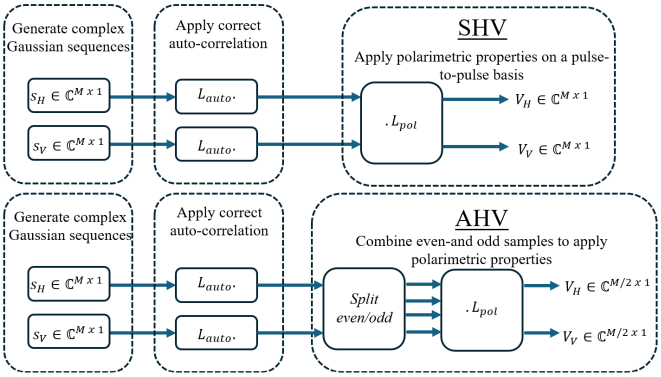

Fig. 2. Simulation flowchart.

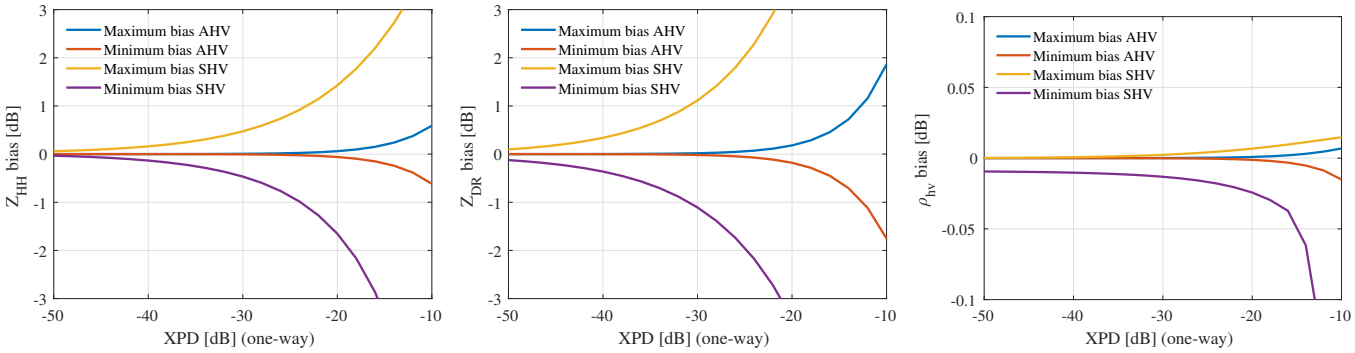

Fig. 3. Bias of the polarimetric variables for different levels of cross-polar discrimination in an S-band rainfall scenario: (a) Horizontal reflectivity, (b) Differential reflectivity, (c) Co-polar correlation coefficient.

The time-series is now simulated according to the flowchart in Fig. 2. In principle, we can construct one random vector containing both H and V samples. The total covariance matrix containing all lags can then be constructed using (11). Mathematically, however, this is equivalent to splitting the simulation into two steps, first generating sequences with the correct autocorrelation resulting from the Doppler spectrum [10], [13], and then combining these sequences to apply the correct polarimetric properties. This is be done by generating two complex random Gaussian white noise sequences. The correct autocorrelation is then applied to these sequences: through filtering [10], [11], Fourier transform techniques [14], or using a decomposition such as the Cholesky method to the covariance matrix constructed from the autocorrelation used [15]. The methods were compared in [15] and, based on the conclusion there, the Cholesky decomposition is utilized here. Afterwards, the correct polarimetric covariance matrix must be applied. The Cholesky decomposition is utilized for this as well, where the covariance matrices are calculated based on (11). For the SHV mode, polarimetric effects are decoupled from Doppler effects, and the matrix can be applied on a pulse-to-pulse basis. For the AHV mode, however, they become coupled. Nonetheless, a process with the correct covariance matrix can be retrieved by combining the even samples of the generated sequences to generate the received co-polar samples when H was transmitted, and the odd samples to generate the received co-polar V samples. The proof is omitted for brevity.

Once the time-series signal is simulated, the polarimetric variables can be estimated. Note that no additive noise was simulated. At signal-to-noise ratios lower than $15\,\mathrm{dB}$, the additive noise can cause additional bias [16], but this is beyond the scope of this paper.

III. Simulation Results

To illustrate the methods described in Section II, an example rainfall event is simulated. The parameters are chosen to match the typical polarimetric signature at S-band [5]. The expected values of the parameters are chosen as:

$$Z_{DR} = 10 \cdot log_{10}\left(\frac{< |s_{hh}|^2 >}{< |s_{vv}|^2 >}\right) = 3\ dB \tag{16}$$

$$L_{DR} = 10 \cdot log_{10}\left(\frac{< |s_{hv}|^2 >}{< |s_{vv}|^2 >}\right) = -25\ dB$$

$$\rho_{hv} \cdot e^{j\Phi_{DP}} = \frac{< s_{hh}^* s_{vv} >}{\sqrt{< |s_{hh}|^2 >< |s_{vv}|^2 >}} = 0.98 e^{j\Phi_{DP}},$$

where Φ_{DP} can be any value, as explained in Section II. The precise value of $< |s_{hh}|^2 >$ (proportional to the horizontal reflectivity) is not important, as all other values are defined relative to it. The correlations of the co-to cross-polar scattering parameters (e.g. $< s_{hh}^* s_{hv} >$) are taken to be zero based on the assumption of reflection symmetry [17].

First, the cross-polarization dependent offsets are calculated, see Fig. 3. The minor differences with [5] are observed because in this work, no approximations are made, and the higher-order terms are taken into account. Differences with [6] are observed due to the fact that in this paper, the "worst-case" offset is calculated across the phase space. It is shown that the AHV mode has a higher tolerance to cross-polar coupling, which is well-established in literature [18]. Interestingly, some asymmetry can be seen between the maximum positive and negative offsets. Requirements on the maximum positive and negative deviation allowed are usually taken to be symmetric [8], even though rain-rate estimation is done using power-law approximations [7, Ch. 8], and its performance is thus not symmetric with regards to positive or negative deviations of the polarimetric variables.

Secondly, the Monte Carlo simulations are carried out based on the time series of the received voltages, to simulate the fluctuations around the maximum positive and minimum negative biases calculated in the previous step. Different values for the total number of echo samples, as well as the normalized spectral width, have to be selected. As shown in [4], [19], it is the ratio between the two that is important. Two cases will therefore be simulated: one where the number of echo samples is very large compared to the inverse of the normalized spectral

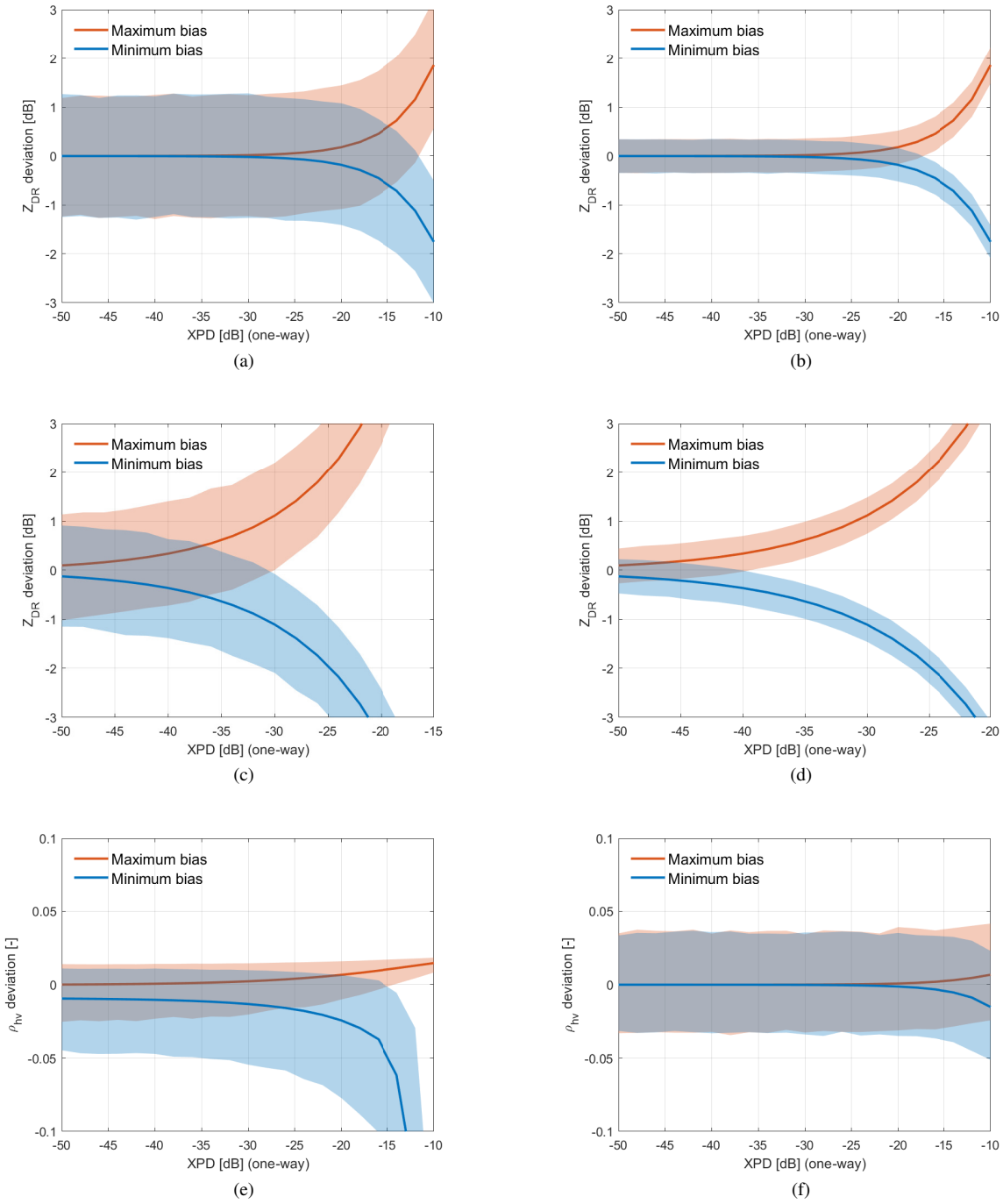

Fig. 4. Deviation bounds for 90 % of cases for different levels of cross-polar discrimination in an S-band rainfall scenario: (a) 16 sample AHV mode differential reflectivity, (b) 128 sample AHV mode differential reflectivity; (c) 16 sample SHV mode differential reflectivity, (d) 128 sample SHV mode differential reflectivity; (e) 16 sample SHV mode co-polar correlation coefficient, and (f) 128 sample AHV mode co-polar correlation coefficient.

width, and one where it is comparable:

$$\text{Case I} : \sigma_{vn} = 0.1 \quad / \quad M = 16,$$
$$\text{Case II} : \sigma_{vn} = 0.1 \quad / \quad M = 128.$$

It should be noted that M denotes the total number of echo samples. In AHV mode, only $\frac{M}{2}$ samples will therefore be available for the estimation. From the resulting distribution, the bounds within which 90 % of the estimates are located are shown. Fig. (4a-4b) and Fig. (4c-4d) show the results for the differential reflectivity in AHV and SHV modes in the two cases, respectively. Comparing the two, it can be seen that the AHV mode has higher cross-polarization tolerance, whereas the estimator spreads are comparable to the SHV mode. The latter can be attributed to the reduction of the bounds does

not scaling linearly with the number of echo samples. This is because of the following: firstly, the samples are correlated, implying the number of independent echo samples is smaller than the total number of samples [7, Ch. 5, pp.270-272]. Secondly, the estimates are not perfectly normally distributed. As for the co-polar correlation coefficient, Fig. 4 shows the results for the AHV mode with 128 samples and the SHV mode with 16 samples. To get comparable spreads of the estimators, the AHV mode thus needs considerably more samples compared to the SHV mode. This is because of the extra uncertainty introduced in the AHV case, as the co-polar correlation coefficient needs to be estimated with a one-lag delay, which implies the samples are already partially decorrelated. To compensate for this effect, an estimate of the autocorrelation coefficient is used, which itself has statistical fluctuations. Though not shown here, this introduces extra bias as well, in the case of a low number of samples and/or a high spectral width [9].

The results were simulated using the MATLAB software, on a system with an Intel i7-13850HX CPU with 32 GB of RAM. Simulation times for the first part, consisting of the cross-polarization dependent offsets, is in the order of a few minutes when the angular search space is discretized by 2 degrees. Simulation times for the Monte Carlo runs are in the order of a few seconds to a minute for 5000 runs.

In general, the rainfall example shows that it is necessary to take into account both the XPD and the number of echo samples and Doppler parameters while defining the requirements. In practical scenarios, the bounds might be reduced by spatially averaging the estimates. This comes, however, at the cost of reduced spatial resolution.

IV. Conclusion

The impact of the finite number of echo samples available in realistic weather radar applications and the cross-polar coupling on the accuracy of polarimetric measurements is investigated. A novel methodology to show the $90\,\%$ bounds within which the estimators will be due to the combination of the aforementioned effects is proposed. Requirements on XPD are shown to become more stringent due to the combination of these effects. It is shown that achieving extremely high XPD comes with diminishing returns, as the increasing cost and complexity are not accompanied by an adequate increase in data quality, which remains limited by the finite number of available echo samples. These findings are illustrated using the proposed methodology for a realistic rainfall scenario. The AHV and SHV modes are compared, and the trade-off between the Doppler-tolerant SHV mode and the XPD-tolerant AHV mode is shown. For example: at an XPD of 30 dB, using 128 samples, it is shown that deviations in differential reflectivity from the true value are as follows. In the AHV mode, considering the worst-case positive bias, deviations are between 0.36 dB and -0.33 dB in $90\,\%$ of the estimates, and these values are mostly influenced by the finite number of samples. In the SHV mode, for the same scenario, deviations are between 0.75 and 1.48 dB, and though the spread is similar, these values are heavily influenced by the bias induced by the cross-polar coupling. For the co-polar correlation coefficient, however, the AHV mode needs 128 samples at an XPD of 30 dB to get comparable data quality to the 16-sample case for the SHV mode, showing its sensitivty to the Doppler properties. Future work will include simulation of other weather scenarios and more complex measurement modes than SHV and AHV.

References

[1] M. R. Kumjian, "Principles and applications of dual-polarization weather radar. part i: Description of the polarimetric radar variables.," *Journal of Operational Meteorology*, vol. 1, 2013.

[2] A. V. Ryzhkov and D. S. Zrnić, *Radar polarimetry for weather observations*. Springer, 2019, vol. 486.

[3] R. J. Doviak, D. S. Zrnic, and R. M. Schotland, "Doppler radar and weather observations," *Applied Optics*, vol. 33, no. 21, p. 4531, 1994.

[4] T. Dash, H. Driessen, O. Krasnov, and A. Yarovoy, "Doppler Spectrum Parameter Estimation for Weather Radar Echoes Using a Parametric Semi-analytical Model," *IEEE Transactions on Geoscience and Remote Sensing*, vol. 62, pp. 1–18, 2024.

[5] Y. Wang and V. Chandrasekar, "Polarization isolation requirements for linear dual-polarization weather radar in simultaneous transmission mode of operation," *IEEE Transactions on Geoscience and Remote Sensing*, vol. 44, no. 8, pp. 2019–2028, 2006.

[6] M. An, J. Yin, T. Wang, and Y. Li, "Quantitative impacts of different polarization operating modes and waveforms on weather observables for polarimetric phased array radar," *IEEE Transactions on Geoscience and Remote Sensing*, 2024.

[7] V. N. Bringi and V. Chandrasekar, *Polarimetric Doppler weather radar: principles and applications*. Cambridge university press, 2001.

[8] V. M. Melnikov and D. Zrnic, "Simultaneous transmission mode for the polarimetric wsr-88d: Statistical biases and standard deviations of polarimetric variables," *NOAA/NSSL Rep*, vol. 84, 2004.

[9] V. M. Melnikov and D. S. Zrnić, "On the alternate transmission mode for polarimetric phased array weather radar," *Journal of atmospheric and oceanic technology*, vol. 32, no. 2, pp. 220–233, 2015.

[10] V. S. D. Rio and M. Vera-Isasa, "A unified formulation of polarimetric weather radar with application to iq data simulation," *IEEE Transactions on Geoscience and Remote Sensing*, vol. 57, pp. 5098–5107, 7 Jul. 2019.

[11] S. Lischi, A. Lupidi, M. Martorella, F. Cuccoli, L. Facheris, and L. Baldini, "Advanced polarimetric doppler weather radar simulator," in *2014 15th International Radar Symposium (IRS)*, IEEE, 2014, pp. 1–6.

[12] L. Liu, V. Bringi, V. Chandrasekar, E. Mueller, and A. Mudukutore, "Analysis of the copolar correlation coefficient between horizontal and vertical polarizations," *Journal of Atmospheric and Oceanic Technology*, vol. 11, no. 4, pp. 950–963, 1994.

[13] G. Galati and G. Pavan, "Computer simulation of weather radar signals," *Simulation Practice and Theory*, vol. 3, no. 1, pp. 17–44, 1995.

[14] D. S. Zrnić, "Simulation of weatherlike doppler spectra and signals," *Journal of Applied Meteorology and Climatology*, vol. 14, no. 4, pp. 619–620, 1975.

[15] I. R. Ivić, "Comparison between weather signal simulation in frequency and time domain," *Journal of Atmospheric and Oceanic Technology*, vol. 39, no. 7, pp. 985–997, 2022.

[16] V. M. Melnikov and D. S. Zrnić, "Autocorrelation and cross-correlation estimators of polarimetric variables," *Journal of Atmospheric and Oceanic Technology*, vol. 24, no. 8, pp. 1337–1350, 2007.

[17] S. Nghiem, S. Yueh, R. Kwok, and F. Li, "Symmetry properties in polarimetric remote sensing," *Radio Science*, vol. 27, no. 05, pp. 693–711, 1992.

[18] D. Zrnić, R. Doviak, G. Zhang, and A. Ryzhkov, "Bias in differential reflectivity due to cross coupling through the radiation patterns of polarimetric weather radars," *Journal of Atmospheric and Oceanic Technology*, vol. 27, no. 10, pp. 1624–1637, 2010.

[19] T. Dash, H. Driessen, O. A. Krasnov, and A. Yarovoy, "Counter-Aliasing Is Better Than De-Aliasing: Application to Doppler Weather Radar With Aperiodic Pulse Train," *IEEE Transactions on Geoscience and Remote Sensing*, vol. 62, pp. 1–17, 2024.